ChemComm

COMMUNICATION

View Article Online
View Journal | View Issue

Cite this: *Chem. Commun.*, 2022, **58**, 5889

Received 18th March 2022,
Accepted 20th April 2022

DOI: 10.1039/d2cc01568d

rsc.li/chemcomm

Dual-photofunctional organogermanium compound based on donor–acceptor–donor architecture†

Aleksandra Nyga, ‡[a] Takahito Kaihara,‡[b] Takumi Hosono,[b] Massimiliano Sipala,[a] Patrycja Stachelek,[c] Norimitsu Tohnai,[b] Satoshi Minakata,[b] Leonardo Evaristo de Sousa,[d] Piotr de Silva,*[d] Przemyslaw Data*[a] and Youhei Takeda*[b]

A dual-photofunctional organogermanium compound based on a donor–acceptor–donor architecture that exhibits thermally activated delayed fluorescence and mechano-responsive luminochromism has been developed. The developed compound was successfully applied as an emitter for efficient organic light-emitting diodes.

Organogermanes have attracted attention in a wide variety of research fields such as organometallic chemistry,[1] biology,[2] and catalysis.[3] In sharp contrast, the utilization of organogermanium compounds and polymers as optoelectronic materials has been rarely exploited.[4–6] For example, tetraaryl germanes and related polymers have been used as host materials for organic light-emitting diodes (OLEDs), by utilizing the high triplet energy and adequate carrier transport capability.[4] Also, a systematic study of blue-emitters based on phenothiaborin-connected acridan analogues with group 14 elements including germanium for non-doped efficient OLEDs has been reported.[5] Given unique characteristics of organogermanes such as a large atomic radius (122 pm), electropositive nature (χ_p = 2.01), and capability of σ–π conjugation, the development of novel Ge-containing organic functional materials would offer us great opportunities to cultivate design principles for a new class of functional materials. Specifically, the diminished σ–π conjugation ability of Ge element when compared with Si allows for higher-energy triplet excited states than the corresponding silicon compounds.[4] Since the triplet energy is a limiting factor for determining the emission color of thermally activated delayed fluorescent (TADF),[7] donor–acceptor (D–A) type organogermanes are promising for realizing high-energy TADF (blue to green).[5]

Herein, we disclose the development of a dual-photofunctional Ge-containing donor–acceptor–donor (D–A–D) type compound **1** (Fig. 1a). Notably, the developed compound represents a rare example of luminescent organogermanium compounds,[5,8] and it nicely shows dual photofunctionality of TADF and mechano-responsive luminochromism.[9] Furthermore, compound **1** serves as the first example of green-TADF emitter based on organogermanium for an efficient OLED device.

The synthetic route to compound **1** is shown in Fig. 1b (for the details, see the ESI†). We initially developed a synthetic method for dihydrophenazagermine **4**, starting from *N*-protected dibromo diarylamine **2**. Dilithiation of **2** followed by trapping with Ph_2GeCl_2 and detaching the *N*-*p*-methoxybenzyl (PMB) group with DDQ afforded **4**. The X-ray diffraction analysis of the single crystal **4**

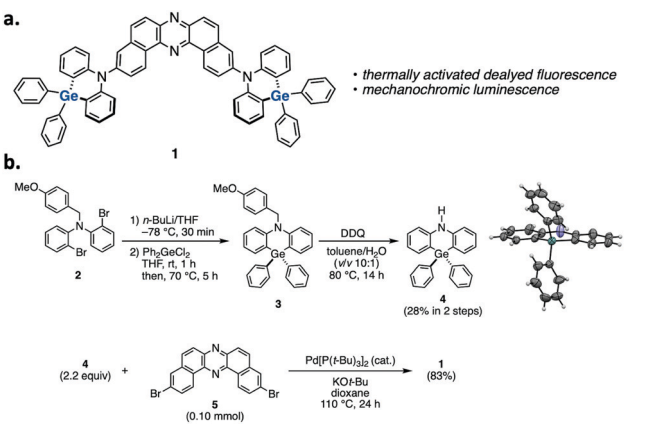

Fig. 1 (a) Structure and (b) synthetic route to compound **1**.

[a] *Faculty of Chemistry, Silesian University of Technology, M. Strzody 9, 44-100, Gliwice, Poland. E-mail: przemyslaw.data@polsl.pl*
[b] *Department of Applied Chemistry, Graduate School of Engineering, Osaka University, Yamadaoka 2-1, Suita, Osaka 565-0871, Japan. E-mail: takeda@chem.eng.osaka-u.ac.jp*
[c] *Chemistry Department, Durham University, South Road, Durham DH1 3LE, UK*
[d] *Department of Energy Conversion and Storage, Technical University of Denmark, Anker Engelunds Vej 301, 2800 Kongens Lyngby, Denmark. E-mail: pdes@dtu.dk*

† Electronic supplementary information (ESI) available: Experimental procedures for the syntheses of materials, spectroscopic data of new compounds, single crystal X-ray crystallographic data, cyclic voltammogram, thermogravimetric analysis (TGA) profiles, the copies of NMR spectra of new compounds, and theoretical calculation details. CCDC 2153796. For ESI and crystallographic data in CIF or other electronic format see DOI: https://doi.org/10.1039/d2cc01568d

‡ These authors contributed equally to this work.

revealed that the angle between two phenylene planes is 173° (the inset figure in Scheme S1, for the details, see Table S1, ESI†), which is larger than that of its Si analogue (*ca.* 133°) in a D–A system.[5] This planar structure of the donor would be ascribed to the longer Ge–C bond (*ca.* 1.93 Å) when compared to Si–C bond (*ca.* 1.85 Å).[5] D–A–D compound **1** was successfully synthesized through a Pd-catalyzed Buchwald–Hartwig amination of 3,11-dibromo-dibenzophenazine **5**[10] with donor **4** (Fig. 1b).

The steady-state UV-vis absorption spectra of diluted solutions ($c = 10^{-5}$ M) of **1** displayed a π–π* absorption at λ_{abs} 300–350 nm and weak vibronic absorption ascribed to the acceptor core at λ_{abs} 380–420 nm (Fig. 2a). Also, in the lower-energy region, a broad and weak absorption ascribed to charge-transfer (CT) transition was observed. In a non-polar solvent (*n*-hexane), compound **1** displayed a vibronically-shaped emission spectrum (λ_{em} 474 nm) with a moderate photoluminescence quantum yield (PLQY), which is ascribed to the emission from the locally excited state (^{1}LE). In contrast to the absorption spectra, the PL spectrum significantly red-shifted as a function of solvent polarity (Fig. 2a), suggesting the CT character of the excited states in those solvents. The Mataga–Lippert plot analysis corroborated the hybridized local and charge-transfer (HLCT) nature of compound **1** (Fig. S3, ESI†). An interesting phenomenon other than solvatochromism involves dual-emission in a polar solvent such as dichloromethane (DCM) and DMF (Fig. 2a). Comparison with a known D–A system

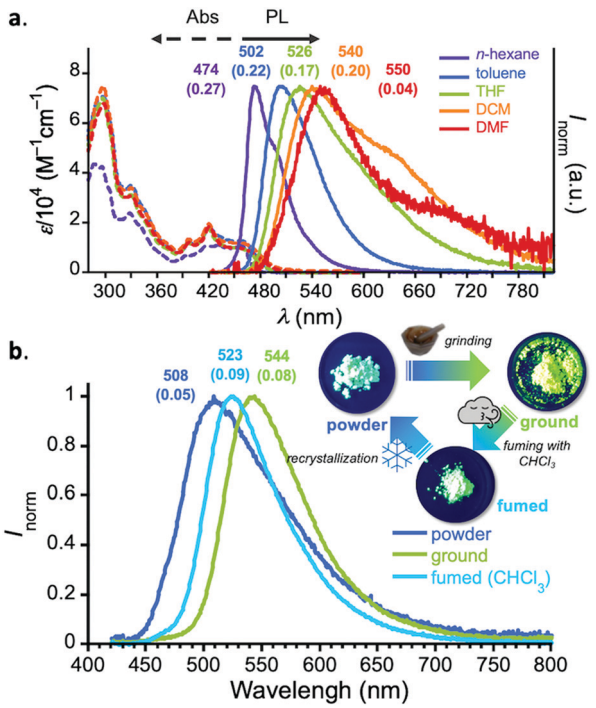

Fig. 2 (a) UV-vis absorption (dotted lines) and PL (solid lines) spectra of diluted solutions of **1** ($c = 10^{-5}$ M). Photoluminescence spectra were acquired with the excitation at λ_{ex} 400 nm. (b) PL spectra of power (blue), ground (moth green), and fumed sample (light blue) of **1** excited at λ_{ex} 400 nm. The photographs represent the image of the emission-color change cycle. All emoji designed by OpenMoji-the open-source emoji and icon project. License: CC BY-SA 4.0.

having a phenazagermin donor allows us to notice that the contribution of the emission ascribed to axial-axial conformer is little in our system.[5] The exclusive population of equatorial-equatorial conformer of compound **1** was supported by the theoretical calculations (*vide infra*).

It is noted that D–A–D compound **1** exhibited a significant change in emission color in the solid states, responding to external stimuli (Fig. 2b). When as-prepared powdery solid ("powder") was ground with a pestle and mortar ("ground"), the emission peak significantly shifted to the lower-energy regime ($\Delta\lambda$ 1303 cm^{-1}). In contrast, when the ground was fumed with organic vapor such as $CHCl_3$ and CH_2Cl_2, the emission spectrum slightly reverted back ($\Delta\lambda$ 738 cm^{-1}). The initial powder state was recovered by recrystallization. The powder X-ray diffraction (PXRD) analyses of the solids revealed that only the peak at $2\theta = 23.4°$ (d = 3.8 Å) significantly decreased upon grinding and its intensity was reverted back upon exposing to chloroform vapor (Fig. S4, ESI†). This would suggest that the emission color change in response to stimuli would be ascribed to the fluctuation of intermolecular electronic interaction.[11] It is noted that such dual photofunctionality of TADF and mechano-responsive emission color change would offer opportunities for sensing applications.[12]

Time-resolved luminescence spectroscopy of compound **1** was performed in both inert non-polar cyclo olefin polymer host Zeonex®, 4,4′-bis(*N*-carbazoyl)-1,1′-biphenyl (CBP), and bis[(2-diphenylphosphino)phenyl]ether oxide (DPEPO) hosts, the latter two of which were used to mimic the chemical environment within an OLED device. Each material showed emission within two distinct time regions within all the hosts. The first, decaying with a lifetime within the nanosecond time regime in all materials, is attributed to prompt emission from the singlet excited state due to its temperature independence (Fig. 3). In all cases, spectral inspection at time delays (TD) = 5 ns shows a Gaussian charge transfer (^{1}CT) singlet peak that decays over longer times.

At longer delay times, in the microsecond/millisecond delay time regions, delayed emission was observed (Fig. 3). Depending upon the experimental temperature, both the singlet state delayed emission and triplet state emission was observed on similar millisecond timescales, and therefore, the emission from each state is most easily elucidated upon spectral inspection at different temperatures (Fig. 3). At room temperature (300 K), the delayed emission spectrum had the same shape and onset energy as the prompt emission in both CBP and DPEPO (Fig. 3c and e). Therefore, the delayed emission was identified as TADF. But, the delayed emission in Zeonex® was observed in a slightly lower-energy region (Fig. 3a), probably due to the structural relaxation in the excited state. Intriguingly, the triplet excited state emissions observed at low temperatures showed quite varied energies: 2.65 eV in Zeonex®, 2.14 eV in CBP, and 2.11 eV in DPEPO hosts (Fig. 3a, c, and e). Such fluctuation in the triplet energy is unusual for dibenzo[*a*,*j*]phenazine-cored D–A–D systems.[13] This observation could suggest a higher triplet state (T_2) was involved in the emission in Zeonex®. Such a scenario was partly supported by the theoretical calculations (*vide infra*). Such complications cause much weaker TADF emission in the CBP and DPEPO

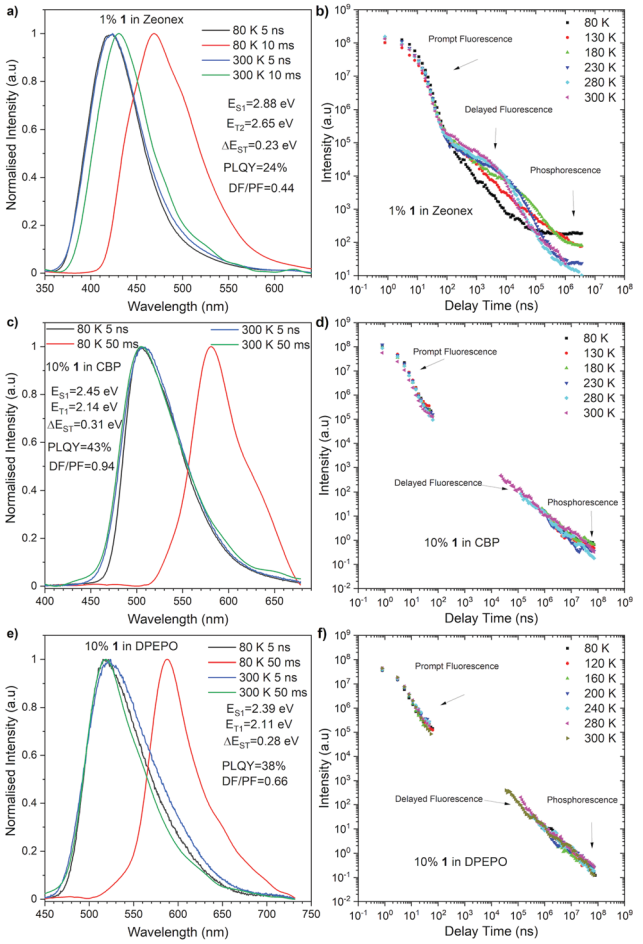

Fig. 3 Emission intensity of **1** against delay time measured in (a) Zeonex®, (c) CBP, and (e) DPEPO at different temperatures. Normalized emission spectra of **1** in (b) Zeonex®, (d) CBP, and (f) DPEPO at varying delay times at 300 K and 80 K.

matrices and a much lower rISC contribution than it was observed in the Zeonex® matrix. The polarity of the host affects the energy of both singlet and triplet excited states. Therefore, as the polarity increases, the ΔE_{ST} of the materials increases from 0.23 eV in Zenex® to 0.31 eV in CBP, and 0.28 in DPEPO, which weaken the rISC process. When compared with the photophysical properties of a phenothiaborine-connected phenazagermine compound[5] in a phosphineoxide host (diphenylphosphoryl)dibenzo[*b*,*d*]furan: PPF, the λ_{em} for **1** in DPEPO (518 nm) locates at the lower-energy region than that for the D–A dyad (468 nm), while the ΔE_{ST} of **1** (0.28 eV) is larger than that for the D–A dyad (0.11 eV).

The OLED devices were fabricated to investigate whether the Ge-containing compound is applicable to optoelectronic applications (Fig. 4). The HOMO and LUMO energy levels of **1** were determined by cyclic voltammetry (CV) to be −5.65 eV and −3.34 eV, respectively (Fig. S1, ESI†). Since the thermogravimetric analysis (TGA) indicated the high thermal stability of compound **1** [T_d (5 wt% loss under N_2) = 466 °C] (Fig. S2, ESI†), the devices were fabricated with thermal evaporation technique. As a result of an optimization study, the optimal configuration was obtained as follows: Device 1

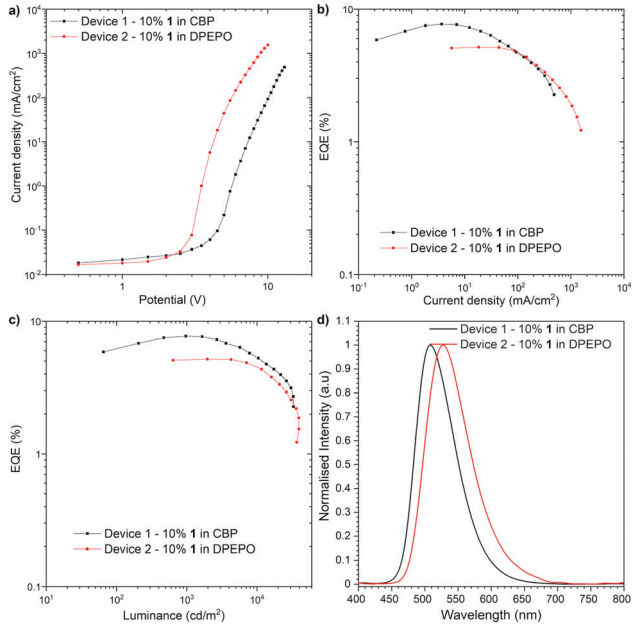

Fig. 4 Device characteristic.

[ITO/*N*,*N*′-di(1-naphthyl)-*N*,*N*′-diphenyl-(1,1′-biphenyl)-4,4′-diamine (NPB) (40 nm)/10% **1** in CBP (25 nm)/2,2′,2″-(1,3,5-benzinetriyl)-tris(1-phenyl-1*H*-benzimida-zole) (TPBi) (40 nm)/LiF (1 nm)/Al (100 nm)], Device 2 [ITO/NPB (40 nm)/tris(4-carbazoyl-9-ylphenyl)amine (TCTA) (10 nm)/10% **1** in DPEPO (20 nm)/TPBi (60 nm)/LiF (1 nm)/Al (100 nm)] (Fig. 4). The characteristics of the OLED structures revealed a good efficiency of Ge-containing TADF emitter **1** in CBP host OLED device (EQE *ca.* 7.7%, Fig. 4b), which exceeds the theoretical maximum of the OLED device fabricated with prompt fluorescent emitter (*ca.* 5%). On the one hand, the DPEPO host-based device showed lower efficiency (EQE *ca.* 5.1%). The luminance of the device in both hosts is quite high (more than 32 000 cd m^{-2} in CBP and 39 000 cd m^{-2} in DPEPO), which suggests good charge recombination in the device. The turn-on voltage was around 2.5 V in DPEPO and 4.0 V in CBP. In both structures, the OLED characteristic showed a moderate roll-off dependency (Fig. 4b and c). It is worth noting that the Ge-containing TADF emitter for OLEDs is quite limited so far,[5] and compound **1** represents the first example of green-TADF emitter based on organogermanium compound.

To obtain further insight into the behavior of compound **1**, density functional theory (DFT) calculations were performed and the nuclear ensemble method was used to estimate photophysical rates[14] (see the ESI† for details). A conformational analysis of **1** was conducted, revealing that the equatorial-equatorial conformation is the most stable one in ground, S_1 and T_1 states. A fluorescence spectrum simulation of compound **1** (Fig. S3, ESI†) predicts an emission peak at 516 nm (2.40 eV) and an emission rate of 1.2×10^7 s^{-1} (Table S5, ESI†), which matches well the experimental value (502 nm) in toluene (Fig. 2) but underestimates the S_1 emission energy in Zeonex® (Fig. 3a), though toluene and Zeonex® share similar dielectric constants (*ca.* 2.3). This suggests that the S_1 emission in this

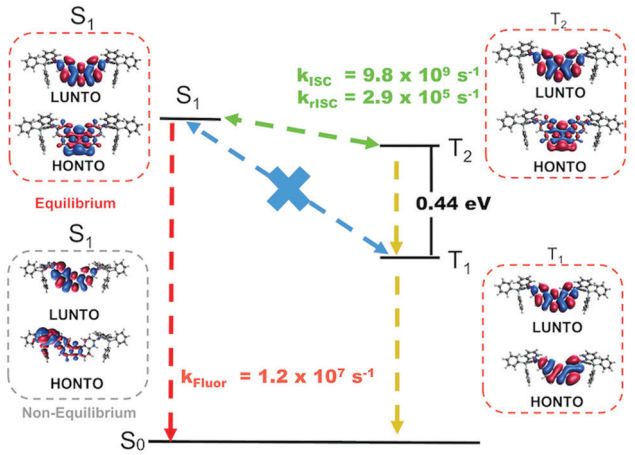

Fig. 5 NTOs for the S_1, T_1 and T_2 states and schematics of the TADF mechanism in compound **1** with DFT estimated rates in toluene. A CT S_1 state calculated at a non-equilibrium geometry is also shown.

case could result from another conformer being preferentially locked in place by solid-state effects specific to this host matrix, a hypothesis that is corroborated by emission energies of 2.83 eV and 2.75 eV calculated for the axial–axial and equatorial–axial conformers, respectively.

Estimated rates for ISC from S_1 (Table S4, ESI†) indicate that the preferred process takes place between the S_1 and T_2 states, due to a lower average energy gap (0.012 eV between S_1 and T_2 *versus* 0.421 eV between S_1 to T_1). The simulated phosphorescence spectra from T_1 and T_2 (Fig. S6 and Tables S4–S6, ESI†) predict one order of magnitude higher emission rate from T_2 than from T_1 with a T_1 peak at 579 nm (2.14 eV) and a T_2 peak at 475 nm (2.61 eV). The predicted energy of T_2 matches the phosphorescence energy measured in Zeonex® (2.65 eV), providing further evidence for the S_1 to T_2 ISC hypothesis. The T_1 energy, in turn, agrees well with phosphorescence energies in CBP and DPEPO (Fig. 3c and e), suggesting that in these host matrices, transfers to T_1 from S_1 may be more efficient due to higher solvatochromic shift or that internal conversion from T_2 can play an important role. In toluene, calculations indicate an average T_1–T_2 gap of 0.44 eV (Table S7, ESI†), enough to prevent rapid depopulation to T_1 if the competing processes (rISC, phosphorescence) are efficient enough. Calculated rISC rates from T_1 and T_2 states (Tables S5 and S6, ESI†) reveal that rISC to S_1 is the preferred transfer for both triplet states. The rISC rate from T_2 to S_1 is orders of magnitude higher than that from T_1, indicating more efficient TADF when T_2 is the state involved in the triplet harvesting mechanism. This agrees with the observed decrease in TADF performance in CBP and DPEPO, which, as mentioned above, have larger T_1 involvement.

Fig. 5 summarizes the proposed TADF mechanism based on the probabilities of each process (Table S8, ESI†). Natural transition orbitals (NTOs) for the S_1, T_1 and T_2 states have mostly localized character, explaining the mild red shift observed from CBP to DPEPO. On the other hand, stronger shifts in solution may result from the fact that vibrational effects can alter the electronic character of the excited states,[15,16] (see example of CT S_1 in Fig. 5) such that the actual picture is not fully captured by NTOs on optimized structures. In fact, this effect should be more prominent in solution than in solid-state, as the vibrational motion may be hindered in the latter case.

In summary, we have developed a dual-photofunctional organogermanium compound that exhibits TADF and mechanochromic behavior. The compound represents the first example of green-TADF emitter using organogermanium scaffold for efficient OLED devices. Theoretical calculations shed light on the importance of the higher triplet excited state to yield TADF *via* rISC process. This work opens up a new avenue for organogermanium-based multi-photofunctional materials in the future.

This work was partly supported by KAKENHI (JP19H05716, JP20H02813, and JP21K18960 to Y. T.), a grant from VILLUM FONDEN (00028053 to P. de Se. and L. E. S.) and the First Team program (POIR.04.04.00-00-4668/17-00 to P. D.). The full list for acknowledgement is included in the ESI.†

Conflicts of interest

There are no conflicts to declare.

Notes and references

1 C. S. Weinert, *Encycl. Inorg. Bioinorg. Chem.*, 2015, 1–18.
2 (*a*) J. S. Thayer, *Appl. Organomet. Chem.*, 1987, **1**, 227–234; (*b*) L. G. Menchikov and M. A. Ignatenko, *Pharm. Chem. J.*, 2013, **46**, 635–638.
3 C. Fricke and F. Schoenebeck, *Acc. Chem. Res.*, 2020, **53**, 2715–2725.
4 (*a*) C. Yao, Q. Cui, J. Peng, X. Xu, R. Liu, J. Wang, Y. Tian and L. Li, *J. Mater. Chem. C*, 2015, **3**, 5017–5025; (*b*) C. Yao, Y. Yang, L. Li, M. Bo, C. Peng and J. Wang, *J. Mater. Chem. C*, 2018, **6**, 6146–6152; (*c*) M.-K. Hung, K.-W. Tsai, S. Sharma, J.-Y. Wu and S.-A. Chen, *Angew. Chem., Int. Ed.*, 2019, **58**, 11317–11323; (*d*) M.-K. Hung, K.-W. Tsai, S. Sharma, J. Lei, J.-Y. Wu and S.-A. Chen, *ACS Appl. Mater. Interfaces*, 2019, **11**, 36895–36904.
5 K. Matsuo and T. Yasuda, *Chem. Sci.*, 2019, **10**, 10687–10697.
6 (*a*) N. Allard, R. B. Aïch, D. Gendron, P.-L. T. Boudreault, C. Tessier, S. Alem, S.-C. Tse, Y. Tao and M. Leclerc, *Macromolecules*, 2010, **43**, 2328–2333; (*b*) J. Ohshita, Y.-M. Hwang, T. Mizumo, H. Yoshida, Y. Ooyama, Y. Harima and Y. Kunugi, *Organometallics*, 2011, **30**, 3233–3236; (*c*) C. M. Amb, S. Chen, K. R. Graham, J. Subbiah, C. E. Small, F. So and J. R. Reynolds, *J. Am. Chem. Soc.*, 2011, **133**, 10062–10065.
7 H. Uoyama, K. Goushi, K. Shizu, H. Nomura and C. Adachi, *Nature*, 2012, **492**, 234–238.
8 (*a*) J. Ohshita, K. Murakami, D. Tanaka, Y. Ooyama, T. Mizumo, N. Kobayashi, H. Higashimura, T. Nakanishi and Y. Hasegawa, *Organometallics*, 2014, **33**, 517–521; (*b*) H. Arii, Y. Iwanami, D. Nakane, H. Masuda, J. Matsumoto, T. Shiragami, K. Mochida and T. Kawashima, *Organometallics*, 2021, **40**, 1363–1370.
9 Y. Sagara, S. Yamane, M. Mitani, C. Weder and T. Kato, *Adv. Mater.*, 2016, **28**, 1073–1095.
10 Y. Takeda, M. Okazaki and S. Minakata, *Chem. Commun.*, 2014, **50**, 10291–10294.
11 S. Goto, Y. Nitta, N. O. Decarli, L. E. de Sousa, P. Stachelek, N. Tohnai, S. Minakata, P. de Silva, P. Data and Y. Takeda, *J. Mater. Chem. C*, 2021, **9**, 13942–13953.
12 P. Data and Y. Takeda, *Chem. – Asian J.*, 2019, **14**, 1613–1636.
13 Y. Takeda, P. Data and S. Minakata, *Chem. Commun.*, 2020, **56**, 8884–8894.
14 L. E. de Sousa and P. de Silva, *J. Chem. Theory Comput.*, 2021, **17**, 5816–5824.
15 L. E. de Sousa and P. de Silva, *ChemRxiv*, 2022, DOI: **10.26434/chemrxiv-2022-pq978**.
16 P. de Silva, C. A. Kim, T. Zhu and T. Van Voorhis, *Chem. Mater.*, 2019, **31**, 6995–7006.

